A New Look at the Binary Interaction: Potential Vorticity Diagnosis of the Unusual Southward Movement of Tropical Storm Bopha (2000) and Its Interaction with Supertyphoon Saomai (2000)

CHUN-CHIEH WU, TRENG-SHI HUANG, WEI-PENG HUANG, AND KUN-HSUAN CHOU

Department of Atmospheric Sciences, National Taiwan University, Taipei, Taiwan

(Manuscript received 28 June 2002, in final form 22 November 2002)

ABSTRACT

Tropical Storm Bopha (2000) showed a very unusual southward course parallel to the east coast of Taiwan, mainly steered by the circulation associated with Supertyphoon Saomai (2000) to Bopha's east. The binary interaction between the two typhoons is well demonstrated by the potential vorticity (PV) diagnosis. With the use of the piecewise PV inversion, this paper quantitatively evaluates how Bopha moved southward due to the binary interaction with Saomai. A newly proposed centroid-relative track, with the position weighting based on the steering flow induced by the PV anomaly associated with the other storm, is plotted to highlight such binary interaction processes. Note that the above analysis can be well used to understand the more complicated vortex merging and interacting processes between tropical cyclones either from observational data or numerical experiments. The results also shed some light on the prediction of nearby tropical cyclones.

1. Introduction

The concept of binary interaction has been well described by tank experiments (Fujiwhara 1921, 1923, 1931), observations (Brand 1970; Dong and Neumann 1983; Lander and Holland 1993; Carr et al. 1997; Carr and Elsberry 1998), and modeling studies (Chang 1983, 1984; DeMaria and Chan 1984; Ritchie and Holland 1993; Holland and Dietachmayer 1993; Wang and Holland 1995), all indicating that two tropical cyclones can interact and then develop mutual orbiting and possible approaching, merging, and escaping processes (Lander and Holland 1993). The binary interaction is not only an interesting and fundamental problem in fluid mechanics and vortex dynamics, but also of practical concern in improving the forecast accuracy of multiple tropical cyclones in close vicinity.

Early laboratory experiments by Fujiwhara (1921, 1931) studied the interaction of binary vortex systems. In addition to the mutual rotational effect, Fujiwhara also detected a tendency for an attraction between vortices having the same sense of rotation. A close meteorological analogy to these laboratory vortices occurs when two tropical cyclones are close sufficiently for mutual interaction. An analytical model by Gryanik (1983) used singular geostrophic vortices to represent localized vortical disturbances. The mutual rotation of interacting hurricanes was qualitatively demonstrated. Observational evidences (Brand 1970) suggested that there is a correlation between the separation distance and the angular rotation rate of two tropical cyclones. Brand also showed that the effect of such a binary interaction depends on differences in storm size and intensity, and on variations in the currents within which the tropical storm systems are imbedded. Specifically, Brand showed that when the distance of two tropical cyclones is under 750 nm (nautical miles), they begin to circle around each other; as the distance is less than 400 nm, they apparently attract each other.

Dong and Neumann (1983) analyzed the best-track data from 1946 through 1981 and showed that the annual frequency of binary interaction is higher (1.5 times) in the western North Pacific than that (0.33 times) in the Atlantic. Dong and Neumann verified mutual interaction of spatially proximate tropical cyclones according to the Fujiwhara expectation, although in some exceptional cases such an effect tends to be masked by other environmental currents.

Lander and Holland (1993) performed a more detailed analysis based on 44-yr data from 1945 through 1988 to observe the behavior of interacting tropical-cyclone-scale vortices in the western North Pacific. Lander and Holland showed that rarely does the interaction of cyclones follow the classic Fujiwhara model. Instead, a series of interactions may occur, including capturing, stable cyclonic orbiting, and cyclone merging and escaping.

Corresponding author address: Dr. Chun-Chieh Wu, Dept. of Atmospheric Sciences, National Taiwan University, 61, Ln. 144, Sec. 4, Keelung Rd., Taipei 106, Taiwan.
E-mail: cwu@typhoon.as.ntu.edu.tw

Many of the above processes have also been closely examined from numerical studies of Ritchie and Holland (1993), Holland and Dietachmayer (1993), and Wang and Holland (1995). Interestingly, a recent observational case study from Kuo et al. (2000) clearly documented a case of interaction and merger of Supertyphoon Zeb and Tropical Storm Alex (1998). It is shown that the two storms rotated around each other when they were within about 850 km, and then the weaker Alex was sheared into a potential vorticity filament by the stronger circulation associated with Zeb, absorbed into Zeb as a rainband.

Concerning the more complicated and realistic flow patterns surrounding tropical cyclones, recent work from Carr et al. (1997) and Carr and Elsberry (1998) has proposed detailed conceptual models to categorize the binary interaction processes, namely, 1) the direct tropical cyclone (TC) interaction with one-way influence, mutual interaction, or merger of the two TCs; 2) the semidirect TC interaction involving another TC and an adjacent subtropical anticyclone; and 3) the indirect TC interaction involving the anticyclone between the two TCs. In spite of their successful rate of 80% in distinguishing the modes of the binary interactions from analyses of 8-yr samples of western North Pacific TCs, it remained unsolved how to quantify the binary interaction of TCs.

Meanwhile, studies (Chan and Gray 1982) have clearly shown that tropical cyclone motion is mainly governed by the tropospheric average steering flow, generally defined as the weighted vertical average of the flow in the troposphere. As an example, during the summer and early autumn seasons tropical cyclones in the western North Pacific generally move westward, northwestward, or northward, mainly driven by the flow associated with the dominant Pacific High to the east or northeast of these storms. Curious enough, Tropical Storm Bopha (2000) moved westward from 7 to 9 September, then had a dramatic southward turn on 9 September, and finally continued its unusual southward course parallel to the east coast of Taiwan until 11 September when it dissipated near the east coast of the Philippines.

It is interesting to ask what led to such an atypical southward track of Bopha. The answer appears empirically and intuitively clear, that is, such motion was likely to be steered by the circulation attributed to Supertyphoon Saomai (2000) to Bopha's east. In other words, the mechanism of the Fujiwhara effect (Fujiwhara 1923) or binary interaction may be the dominant driving force. However, the question is how we can quantify such an effect. As shown by Dong and Neumann (1983), the effects from the environmental flow need to be filtered out before the real Fujiwhara effect can be determined. With the successful development and application of the piecewise potential vorticity (PV) inversion (Davis and Emanuel 1991; Wu and Emanuel 1995a,b; Shapiro 1996; Shapiro and Franklin 1999), one can quantitatively identify the balanced flow associated with each individual PV anomaly. Therefore, in this paper we shall quantitatively investigate the movement of Bopha, as affected by the presence of Saomai, from the PV diagnosis. The minor steering effect of Typhoon Wukong on Bopha, as well as Bopha on Saomai, is also discussed.

2. Data and methodology

a. Data

The data used in this study are based on the analysis fields of the Global Forecast System (GFS) from the Central Weather Bureau (CWB) in Taiwan, which has a horizontal resolution of 2.5° × 2.5°, and 16-vertical-layer on standard pressure surfaces. The GFS (Liou et al. 1997) is a T79 primitive equation model with 18 sigma levels. The observational data is assimilated into the GFS by the optimal interpolation, while the nonlinear normal-mode initialization was adopted for the initialization of the GFS. Parameterization processes include the 1.5-order eddy-mixing parameterization, shallow convection parameterization, and Arakawa–Schubert Cumulus parameterization (Arakawa and Schubert 1974). In addition, the grid-scale latent heating and the radiation of both long- and shortwaves related to clouds are also taken into account.

b. Methodology

1) CONCEPT OF THE PV INVERSION

The use of PV for understanding the evolution of the dynamical system in the atmosphere has been well reviewed in Hoskins et al. (1985). Such merit is particularly enhanced with its inversion characteristics. The PV invertibility principle states that given a distribution of PV, a prescribed balanced condition, and boundary conditions, the balanced mass and wind fields can be recovered. The use of the inversion of the quasigeostrophic PV is limited to fluids with a low Rossby number. Using the nonlinear balanced condition (Charney 1955) to invert the Ertel PV, Davis and Emanuel (1991), and Wu and Emanuel (1995a,b) were able to quantitatively examine extratropical cyclogenesis and the steering of tropical cyclones, individually. Formulated on the $\pi[\pi = C_p(p/p_0)^\kappa]$ coordinate and spherical coordinates, the two equations to be solved are

$$q = \frac{g\kappa\pi}{p}\left[(f + \nabla^2\Psi)\frac{\partial^2\Phi}{\partial\pi^2} - \frac{1}{a^2\cos^2\phi}\frac{\partial^2\Psi}{\partial\lambda\partial\pi}\frac{\partial^2\Phi}{\partial\lambda\partial\pi} - \frac{1}{a^2}\frac{\partial^2\Psi}{\partial\phi\partial\pi}\frac{\partial^2\Phi}{\partial\phi\partial\pi}\right], \quad \text{and} \tag{1}$$

$$\nabla^2\Phi = \nabla\cdot(f\nabla\Psi) + \frac{2}{a^4\cos^2\phi}\frac{\partial(\partial\Psi/\partial\lambda, \partial\Psi/\partial\phi)}{\partial(\lambda, \phi)}, \tag{2}$$

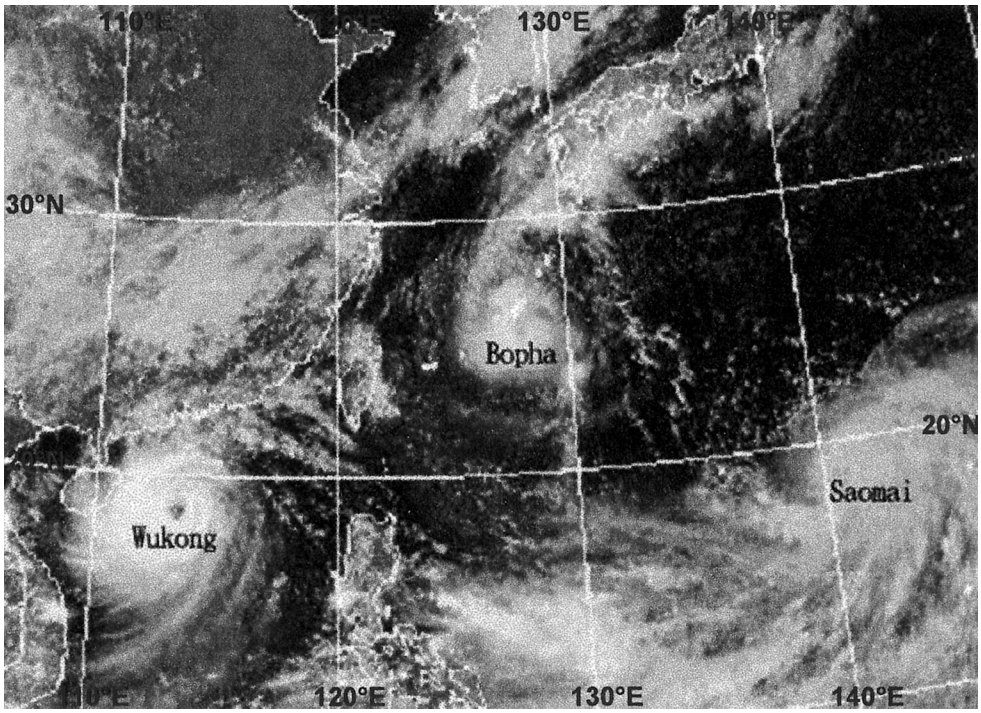

FIG. 1. Japanese GMS imagery at 0600 UTC 8 Sep 2000. The three tropical cyclones are Wukong, Bopha, and Saomai from the left to the right.

where "q" stands for PV, Φ for geopotential height, Ψ for streamfunction, "a" for earth's radius, "f" for the Coriolis parameter, $\kappa = R_d/C_p$, λ for longitude, and ϕ for latitude. Given the distribution of q, the lateral boundary of Φ and Ψ, and the θ ($\theta = -\partial\Phi/\partial\pi$) on the upper and lower boundaries, the distribution of Φ and Ψ can be solved using the successive over- and under-relaxation method (see Davis and Emanuel 1991). Therefore, the nondivergent wind and potential temperature can also be obtained by the following two relations:

$$\mathbf{V} = \hat{k} \times \nabla\Psi \quad \text{and} \quad \theta = -\frac{\partial\Phi}{\partial\pi}.$$

Another robust strength associated with inversion of PV is the so-called piecewise PV inversion, that is, when the flow field is appropriately divided into the mean and perturbation components, the above equations can be rederived (Davis 1992) to obtain the balanced fields associated with each individual PV perturbation. Such methods provide a succinct approach to understanding how the dynamical systems (PV fields) interact with each other in the real atmosphere, and how the tropical cyclone track is affected by different PV features in the observational data (Wu and Emanuel 1995a,b; Shapiro 1996; Shapiro and Franklin 1999), and in the modeling atmosphere (Wu and Kurihara 1996).

2) THE SHAPIRO (1996) DECOMPOSITION

Note that how one chooses the appropriate mean field for piecewise inversion depends on the problems to be tackled. In Wu and Emanuel (1995a,b), the climatological average was taken as the mean field while the piecewise PV inversion was performed. Therefore, the decomposition between the perturbation and the tropical cyclone vortex was complicated. Wu and Emanuel suggested that a clear-cut approach be required to partition the axisymmetric component of the tropical cyclone vortex from its perturbation.

Shapiro (1996) devised a new decomposition by taking the axisymmetric vortex as the mean field and the rest as the perturbation, and such decomposition could clearly demonstrate how the environmental perturbation interacts with the tropical cyclone vortex.

In this research, to understand how Bopha was steered southward by the perturbation flow field (such as those associated with the vortex of Saomai), we take the axisymmetric average relative to the center of Bopha as the mean part, and then follow the approach of Shapiro (1996) to perform the piecewise PV inversion. In other words, we first construct the azimuthal average of the wind field to obtain the average streamfunction $\overline{\Psi}$, so that the associated average geopotential height can be derived from the nonlinear balance equation,

$$\nabla^2\hat{\Phi} = \nabla \cdot (f_0\nabla\overline{\Psi}) + \frac{2}{a^4\cos^2\phi}\frac{\partial(\partial\overline{\Psi}/\partial\lambda,\ \partial\overline{\Psi}/\partial\phi)}{\partial(\lambda,\ \phi)}. \quad (3)$$

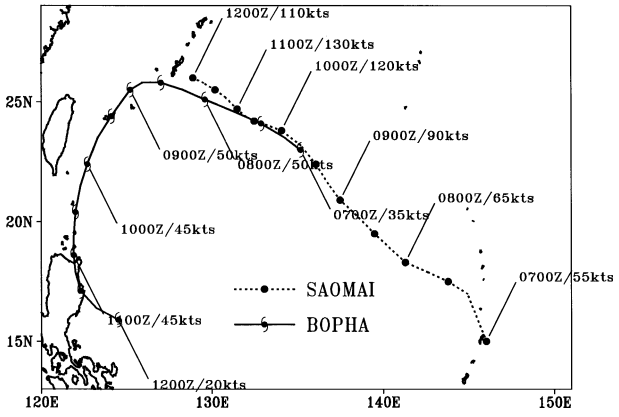

FIG. 2. Best tracks of Bopha (solid line) and Saomai (dotted line) from JTWC for every 12-h from 0000 UTC 7 Sep to 0000 UTC 12 Sep 2000. The maximum surface wind speed (in kt; from JTWC) is also indicated.

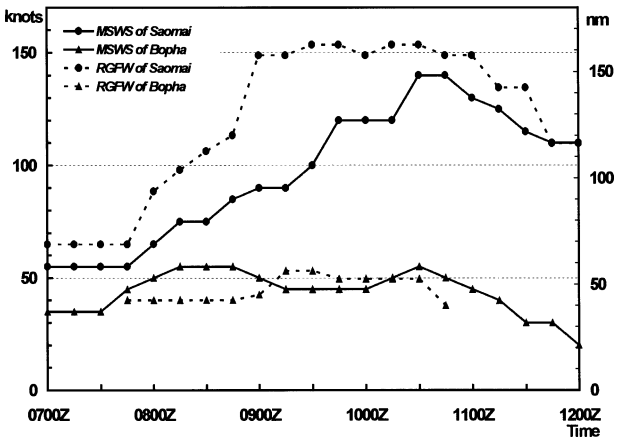

FIG. 3. The time evolution of maximum surface wind speed (kt; from JTWC; denoted as MSWS) and radius of gale-force wind (nm; all-quadrant average from JTWC; denoted as RGFW) of Bopha and Saomai from 0000 UTC 7 Sep to 0000 UTC 12 Sep 2000.

The averaged PV field is then calculated by the following relation:

$$\hat{q} = \frac{gk\pi}{p}\left[(f + \nabla^2\overline{\Psi})\frac{\partial^2\hat{\Phi}}{\partial\pi^2} - \frac{1}{a^2\cos^2\phi}\frac{\partial^2\overline{\Psi}}{\partial\lambda\partial\pi}\frac{\partial^2\hat{\Phi}}{\partial\lambda\partial\pi} - \frac{1}{a^2}\frac{\partial^2\overline{\Psi}}{\partial\phi\partial\pi}\frac{\partial^2\hat{\Phi}}{\partial\phi\partial\pi}\right]. \quad (4)$$

By taking the perturbation field as $\psi' = \psi - \overline{\psi}$, $\Phi' = \Phi - \hat{\Phi}$, and $q' = q - \hat{q}$, the piecewise PV inversion can be performed to calculate the balanced flow and mass fields associated with each PV perturbation. In this study, to show how the flow field attributed to Saomai affected the motion of Bopha, the whole PV perturbation (q') is divided into two parts: one is the PV anomaly associated with Saomai (q'_s, see the distinct feature of shaded positive PV anomaly associated with Saomai in Fig. 7); the other is associated with the environmental PV perturbation except for Saomai ($q'_{\rm ns}$). Note that by definition, $q' = q'_s + q'_{\rm ns}$. Meanwhile, to evaluate the effect of Wukong on the motion of Bopha, the flow associated with the PV perturbation of Wukong (q'_w, see Fig. 6) is also inverted. On the other hand, similar piecewise PV inversion procedures have also been performed to evaluate the impact of the PV perturbation of Bopha (q'_b) on Saomai (note that in this occasion the axisymmetric average relative to the center of Saomai is taken as the mean part).

3. Results

a. Synopsis of Bopha

Tropical storm Bopha had a very unusual track for tropical cyclones in the western North Pacific in 2000. Bopha formed several miles to the southeast of Okinawa and ahead of the intensifying Saomai, while a third typhoon, Wukong, was located over South China Sea (Fig. 1). Bopha moved west-northwestward and passed by Okinawa just as Saomai began rapidly deepening into a supertyphoon. As shown in Fig. 2 [best-track analyses from Joint Typhoon Warning Center (JTWC)], while Saomai continued moving northwestward, the large circulation associated with the intense Saomai (see the later discussion on Fig. 3) drove Bopha on a very atypical southward course parallel to the east coast of Taiwan and eventually moved into northern Luzon, where it weakened due to the increasingly stronger vertical shear (G. Padget 2001, personal communication; see discussions in the next section related to Fig. 8a).

The time evolution of the maximum surface wind speed and the all-quadrant-averaged radius of gale-force wind (from JTWC) of Bopha and Saomai are shown in Fig. 3. While Bopha remained steady with about constant intensity and size from 7 to 11 September, the intensity and size of Saomai kept increasing with time, and stayed at its peak value from 9 to 10

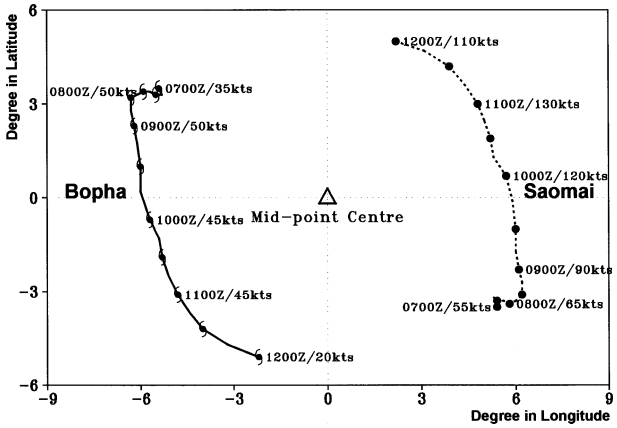

FIG. 4. Relative rotation diagram of 12-h positions relative to the midpoints between Bopha (in solid typhoon symbol) and Saomai (in solid dot) based on a direct binary interaction interpretation.

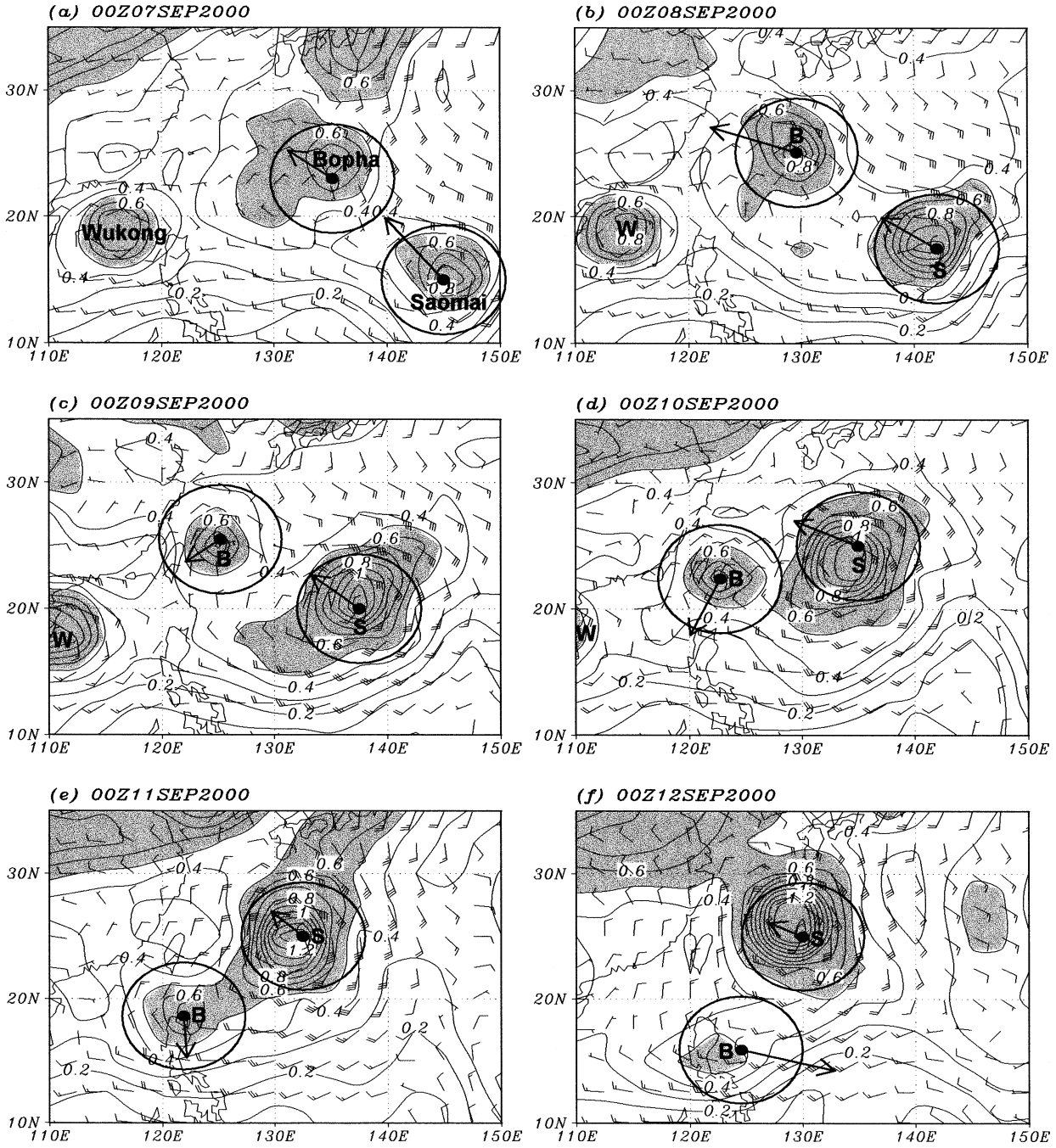

FIG. 5. Potential vorticity (contour interval of 0.1 PVU; PV larger than 0.5 PVU is shaded) at 500 hPa, and the 925–400-hPa deep-layer-mean wind (one full wind barb = 5 m s^{-1}) at 0000 UTC: (a) 7 Sep, (b) 8 Sep, (c) 9 Sep, (d) 10 Sep, (e) 11 Sep, and (f) 12 Sep 2000. The instantaneous movement of Bopha, as well as Saomai, is indicated by the bold arrow, whose length represents the actual translation velocity, and the bold circle shows the scale of 5 m s^{-1}. ''B,'' ''S,'' and ''W'' indicate the PV features of Bopha, Saomai, and Wukong, respectively.

September. The maximum surface wind speed of Bopha (Saomai) is 55 (140) kt, while the largest all-quadrant averaged radius of gale-force wind of Bopha (Saomai) is 60 (155) nm. Apparently Saomai was stronger and larger than Bopha.

The relative motion of Bopha and Saomai in Fig. 2 suggests that they might be under binary interaction. When the relative motion of Bopha and Saomai is plotted with respect to the midpoint between the two TCs (Fig. 4), the result shows quite symmetrically mutual rotating tracks. However, as discussed in Fig. 19 in Carr et al. (1997), this type of relative rotation diagram can

be misleading to the physical mechanisms leading to track alteration, since it is unreasonable to expect the weaker and smaller Bopha would cause a significant orbiting motion of the larger and stronger Saomai. It would make more sense to envision that both TCs, though uneven in strength and size, rotate around their centroid. Considering that Saomai was much stronger and larger, the centroid should be closer to Saomai, the relative rotation of Bopha with respect to Saomai would have been much larger. A way of identifying the centroid of two interacting storms is proposed in the next section to highlight the binary interaction processes.

b. PV diagnosis

Figure 5 shows the potential vorticity (q) and wind fields at 500 hPa and the steering flow ($\mathbf{V}_{\rm SDLM}$), defined as the deep-layer-mean (925–400 hPa) wind vector (in bold arrow) averaged over the inner 3° latitude around each storm center, that is, the steering wind at each level is

$$\mathbf{V}_S(p) = \frac{\int_0^{3^\circ}\int_0^{2\pi} \mathbf{V} r\, dr\, d\theta}{\int_0^{3^\circ}\int_0^{2\pi} r\, dr\, d\theta}, \tag{5}$$

and the 925–400-hPa deep-layer-mean steering wind is

$$\mathbf{V}_{\rm SDLM} = \frac{\int_{925\ \rm hPa}^{400\ \rm hPa} \mathbf{V}_S(p)\, dp}{\int_{925\ \rm hPa}^{400\ \rm hPa} dp}. \tag{6}$$

At 0000 UTC 7 September (Fig. 5a), Bopha and Saomai were both located in a region of high PV, with maximum PV of about 0.7 and 0.8 PVU (1 PVU = 10^{-6} m^2 s^{-1} K kg^{-1}), respectively. Meanwhile, moving westward over the South China Sea, Wukong (with 0.7 PVU) remained distant from Bopha. The intensity of Bopha increased slightly in the next 24 h (Figs. 3 and 5b), but then its size (such as the radius of gale-force wind in Fig. 3, and the area encompassed by the contour of 0.5 PVU in Fig. 5) kept shrinking in the next two days, while the intensity and size of Saomai kept increasing (from 0.9 to 1.5 PVU) and became more organized and robust. It is obvious from Fig. 5 that the intensity and size of Saomai were so dominant over Bopha that Bopha exhibited more movement due to the binary interaction.

Based on the partition as indicated in section 2, the perturbation PV (q') and 925–400-hPa deep-layer-mean perturbation wind fields are shown in Fig. 6. In Fig. 6, the mean PV associated with Bopha ($\hat{q}$) has been removed. Therefore, there is no PV signal on Bopha. On the other hand, Fig. 6 clearly shows how the PV perturbation associated with Saomai evolved with time, and how its associated flow might have affected the motion of Bopha.

When only the balanced flow field associated the PV perturbation of Saomai (q'_s) was inverted (Fig. 7), we can calculate its related steering flow [$\mathbf{V}_{\rm SDLM}(q'_s)$] as defined by Eqs. (5) and (6), and see how the motion of Bopha was affected by Saomai. On 7 and 8 September (Figs. 7a,b), as Saomai was still not strong enough, Bopha moved westward, not much affected by the circulation of Saomai. However, from 9 September, as Bopha began to turn southwestward and southward, its motion was more in parallel to the balanced flow associated with Saomai (Figs. 7c–f).

In Fig. 8a, the time series of the deep-layer-mean steering flow associated with each PV perturbation is compared with the actual movement of Bopha. The balanced flow associated with the total perturbation PV [$\mathbf{V}_{\rm SDLM}(q')$] is in good agreement with the motion of the best track [estimated from the 12-h best-track positions, that is, $\mathbf{V}_{\rm BT} = (\mathbf{X}_{t+6h} - \mathbf{X}_{t-6h})/12h$]. The above result indicates that the motion of Bopha was well represented by the deep-layer-mean steering wind field in GFS based on the PV inversion. Note that by design of the piecewise PV inversion, the summation of the balanced flows associated with q'_s and $q'_{\rm ns}$ are identical to the balanced flow associated with q'. The comparison of the balanced flow associated with q'_s and $q'_{\rm ns}$ thus provides clear evidence of how the motion of Bopha was affected by the presence of Saomai. As indicated in Fig. 8a, from 7 to 8 September, the steering due to q'_s was much weaker than due to $q'_{\rm ns}$. However, from 9 September, the motion of Bopha was mainly dominated by the flow field associated with Saomai (q'_s), that is, Saomai contributed a steering of about 7 m s^{-1} from the north. Figure 8a clearly demonstrates how Somai caused the southward motion of Bopha. In other words, the PV diagnosis provides a powerful tool to succinctly distinguish the flow field between the environment and Saomai, and thus can well detect the binary interaction of Saomai and Bopha.

Note that similar piecewise PV inversion has also been done to show the balanced deep-layer-mean steering flow associated with Wukong [$\mathbf{V}_{\rm SDLM}(q'_w)$] on Bopha. Our result (Fig. 8a) indicates that Wukong was too far away from Bopha to have any significant influence. Likewise, we have also done similar analyses to show how the PV perturbation associated with Bopha (q'_b) affected the motion of Saomai. Our results (Fig. 8b) demonstrate that the steering flow [$\mathbf{V}_{\rm SDLM}(q'_b)$] associated with Bopha was rather weak and can only play a minor role in affecting the motion of Saomai.

The vertical shear between 400 and 850 hPa can also be defined as [$\mathbf{V}_{S400}(q') - \mathbf{V}_{S850}(q')$]. The top row of Fig. 8a clearly indicates that a weak 2–3 m s^{-1} shear was present in the first two days between 7 and 9 September. However, the shear became stronger with time, and an easterly shear of about 10 m s^{-1} existed at 1200 UTC 11 September, consistent with the weakening of Bopha as discussed in section 3a.

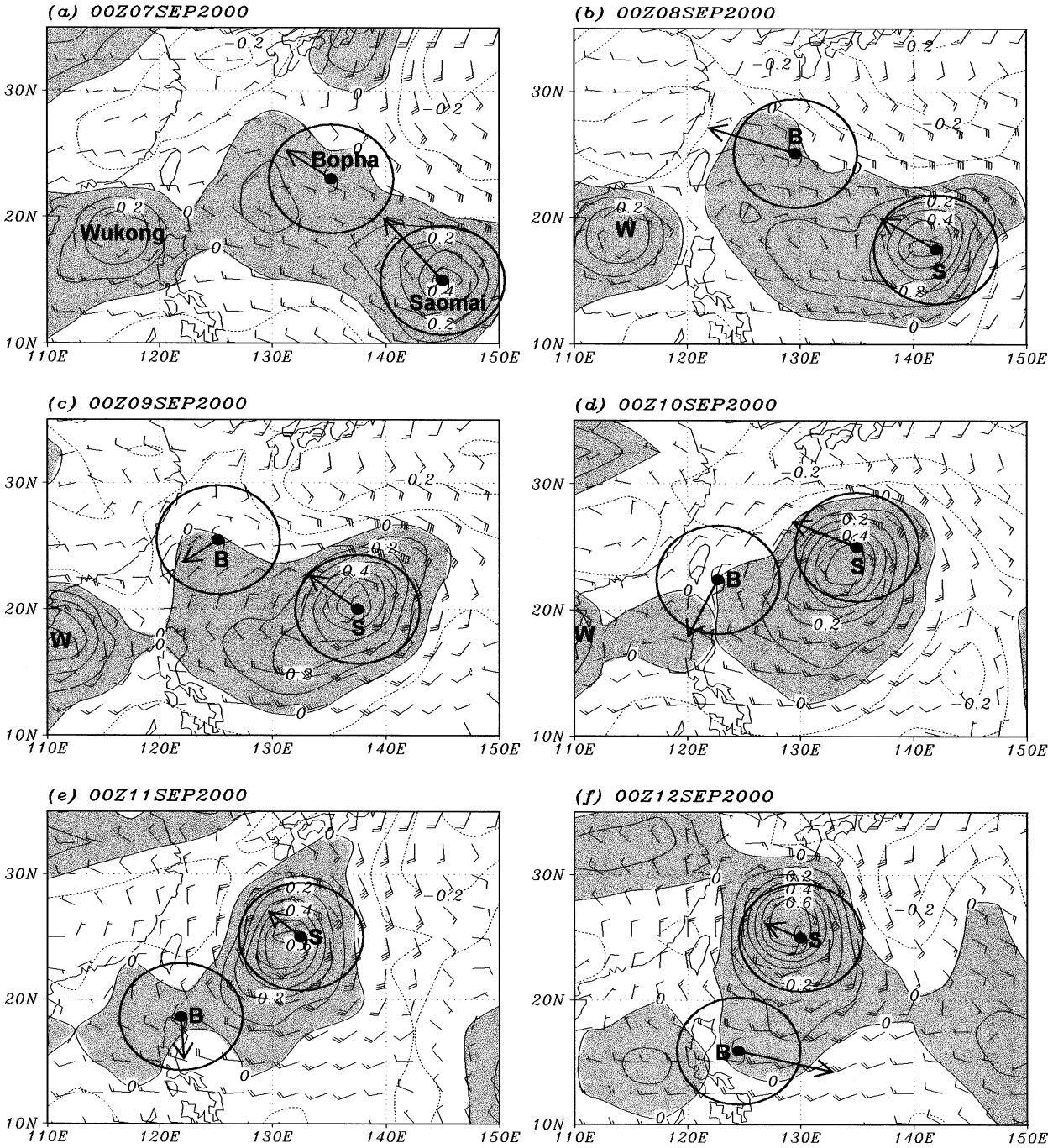

FIG. 6. Potential vorticity perturbation of q' (contour interval of 0.1 PVU; the positive PV perturbation is shaded) at 500 hPa, and the 925–400-hPa deep-layer wind (one full wind barb = 5 m s^{-1}) at 0000 UTC: (a) 7 Sep, (b) 8 Sep, (c) 9 Sep, (d) 10 Sep, (e) 11 Sep, and (f) 12 Sep 2000. The definitions of the bold arrows and circles are as in Fig. 5.

c. Quantification of the binary interaction based on the PV diagnosis

1) DEFINING AT: THE NORMALIZED STEERING EFFECT ASSOCIATED WITH EACH PV PERTURBATION IN THE ALONG-TRACK DIRECTION

The above analyses can also be quantified in Table 1. It is shown that the total steering flow associated with q' [$\mathbf{V}_{\mathrm{SDLM}}(q')$] is very close to the motion vector of the best track ($\mathbf{V}_{\mathrm{BT}}$) in all analysis time. The difference in speed/direction is generally quite small in all time periods, with an average different translation speed (standard deviation; std dev) of -0.03 m s^{-1} (1.04 m s^{-1}), and average different heading direction (std dev) of $-5°$ (18°). To quantitatively measure the influence of the

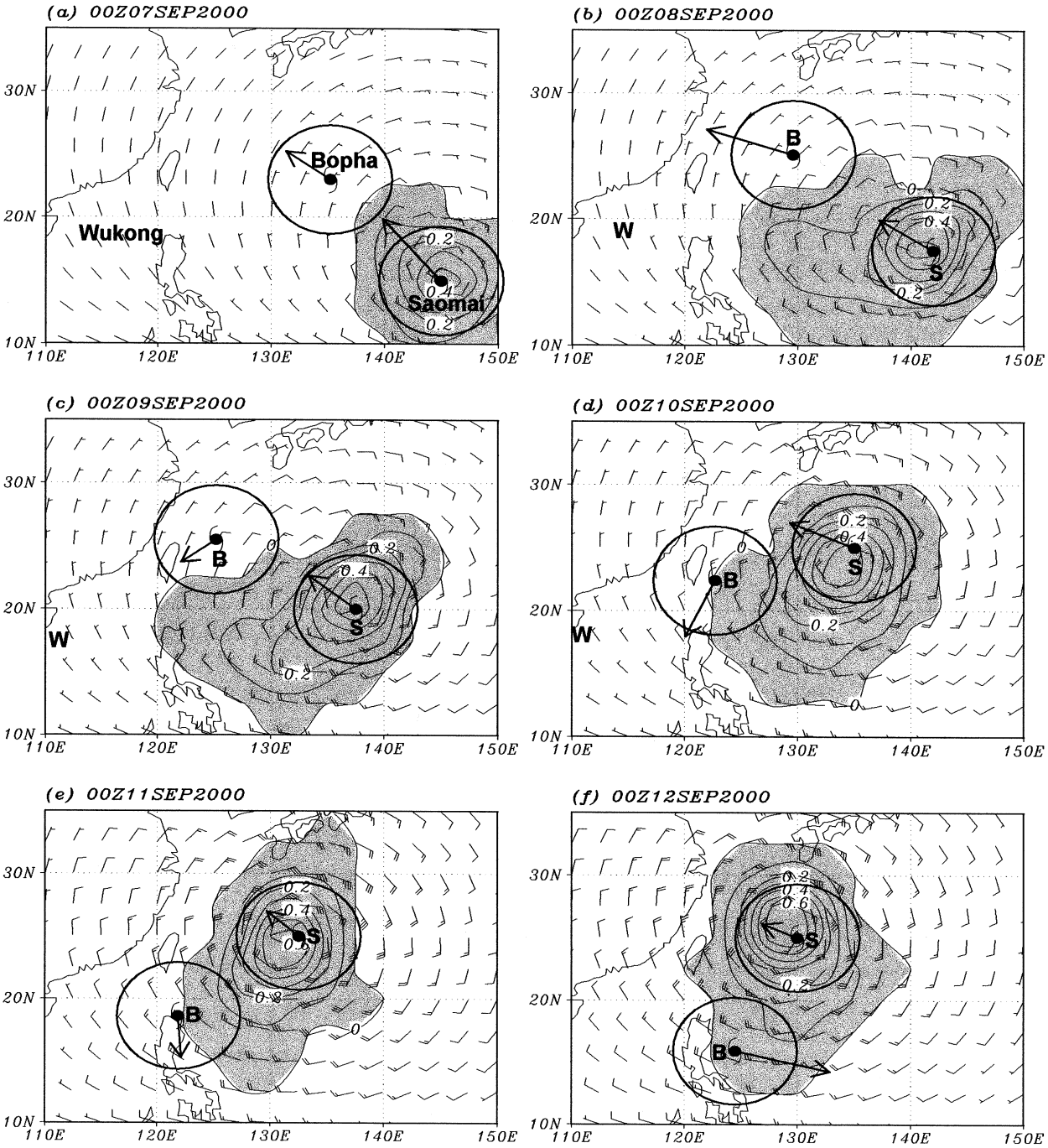

FIG. 7. Potential vorticity perturbation associated with Saomai (q_s') (contour interval of 0.1 PVU; the positive PV perturbation is shaded) at 500 hPa, and the balanced 925–400-hPa deep-layer-mean steering wind [$\mathbf{V}_{\mathrm{SDLM}}(q_s')$; one full wind barb = 5 m s^{-1}] associated with q_s' at 0000 UTC: (a) 7 Sep, (b) 8 Sep, (c) 9 Sep, (d) 10 Sep, (e) 11 Sep, and (f) 12 Sep 2000. The definitions of the bold arrows and circles are as in Fig. 5.

steering flow associated with q_s', the component of the steering flow associated with q_s' [i.e., $\mathbf{V}_{\mathrm{SDLM}}(q_s')$] in the direction parallel to the best-track motion vector ($\mathbf{V}_{\mathrm{BT}}$) (i.e., along-track component) normalized by the best-track speed is calculated, that is,

$$\mathrm{AT}(q_s') = \frac{\mathbf{V}_{\mathrm{SDLM}}(q_s') \cdot \mathbf{V}_{\mathrm{BT}}}{|\mathbf{V}_{\mathrm{BT}}|^2}.$$

Note that by definition, $\mathrm{AT}(q') = \mathrm{AT}(q_s') + \mathrm{AT}(q_{\mathrm{ns}}')$, and a value of one means that the along-track component

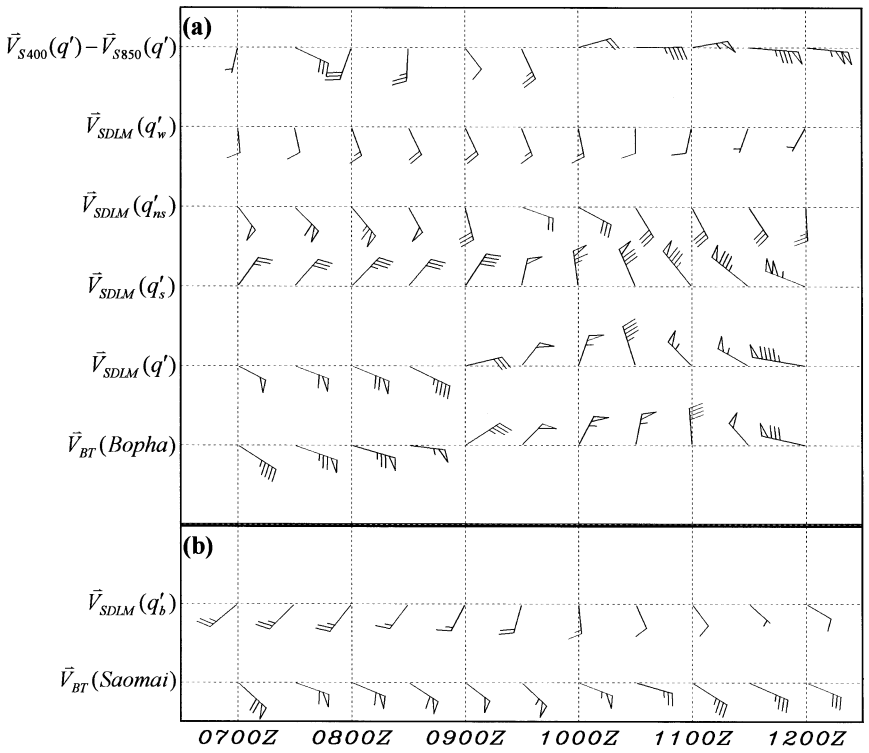

FIG. 8. (a) The movement of Bopha [$\mathbf{V}_{BT}$(Bopha)] and the deep-layer-mean steering flow (averaged in the inner 3° latitude between 925 and 400 hPa) associated with the total PV perturbation [$\mathbf{V}_{SDLM}(q')$], the PV perturbation of Saomai [$\mathbf{V}_{SDLM}(q'_s)$], the PV perturbation other than Saomai [$\mathbf{V}_{SDLM}(q'_{ns})$] (i.e., the environmental PV perturbation except for Saomai), and the PV perturbation of Wukong [$\mathbf{V}_{SDLM}(q'_w)$] for every 12 h from 0000 UTC 7 Sep to 0000 UTC 12 Sep 2000. Here [$\mathbf{V}_{S400}(q') - \mathbf{V}_{S850}(q')$] indicates the vertical shear between 400 and 850 hPa. (b) The movement of Saomai and the deep-layer-mean steering flow associated with the PV perturbation of Bopha [$\mathbf{V}_{SDLM}(q'_b)$]. One full wind barb represents 1 m s^{-1}.

of the steering flow induced by the PV perturbation is identical to the actual storm motion. It is found from Table 1 that the mean value (std dev) of AT (q') is 0.97 (0.2), again indicating the deep-layer-mean steering flow associated with the total PV perturbation provides a good approximation of the actual motion of Bopha. Meanwhile, during the first two days, AT (q'_s) is near zero, while AT (q'_{ns}) remains at about 0.7, indicating the Saomai is not a factor in steering Bopha at this stage. Nevertheless, starting from 0000 UTC 9 September, the value of AT (q'_s) increases to about one as the influence of Saomai on Bopha keep increasing, and becomes lager than 1.5 after 1200 UTC 10 September. Consistent with the result shown in Fig. 8a, apparently Saomai played the dominant role in advecting Bopha southward. On the other hand, the value of AT (q'_w) is most of the time smaller than 0.3, indicating that the motion of Bopha is less affected by the presence of Wukong. Interestingly, the negative value of AT (q'_w) at later time periods shows that the flow associated with Wukong steered Bopha northward. Similarly, the value of AT (q'_b) is about 0.3 or smaller (see the far-right three columns in Table 1), indicating that the influence of Bopha on Saomai is rather limited.

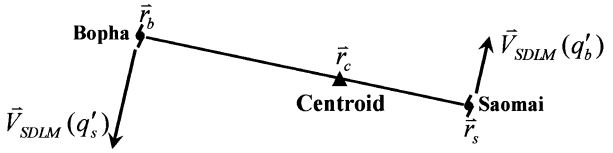

$$\vec{r}_c = \frac{|\vec{V}_{SDLM}(q'_b)|}{|\vec{V}_{SDLM}(q'_s)| + |\vec{V}_{SDLM}(q'_b)|}\vec{r}_b + \frac{|\vec{V}_{SDLM}(q'_s)|}{|\vec{V}_{SDLM}(q'_s)| + |\vec{V}_{SDLM}(q'_b)|}\vec{r}_s$$

FIG. 9. Schematic diagram of the definition of the location of the centroid ($\mathbf{r}_c$) between Bopha ($\mathbf{r}_b$) and Saomai ($\mathbf{r}_s$).

2) DEFINING THE NEW CENTROID FOR PLOTTING THE CENTROID-RELATIVE TRACKS

The centroid-relative tracks are often plotted to illustrate the effect of the binary interaction. For idealized vortices (such as Rankine vortices of singular vortex), it is not difficult to identify the centroid of two vortices based on the strength and the circulation

TABLE 1. The comparison of $\mathbf{V}_{BT}$ (Bopha), $\mathbf{V}_{SDLM}(q')$, the difference [DIF (Bopha)] between $\mathbf{V}_{BT}$ (Bopha) and $\mathbf{V}_{SDLM}(q')$, $\mathbf{V}_{SDLM}(q'_s)$, $\mathbf{V}_{SDLM}(q'_{ns})$, and $\mathbf{V}_{SDLM}(q'_w)$ (in speed/direction). The values of AT (q'_s), AT (q'_{ns}), and AT (q'_w) are also shown. The three far-right columns show the comparison of $\mathbf{V}_{BT}$ (Saomai), $\mathbf{V}_{SDLM}(q'_b)$, and the value of AT (q'_b).

Time (UTC)	$\mathbf{V}_{BT}$ (Bopha) (m s^{-1}/°)	$\mathbf{V}_{SDLM}(q')$ (m s^{-1}/°)	DIF (Bopha) (m s^{-1}/°)	AT (q')	$\mathbf{V}_{SDLM}(q'_s)$ (m s^{-1}/°)	AT (q'_s)	$\mathbf{V}_{SDLM}(q'_{ns})$ (m s^{-1}/°)	AT (q'_{ns})	$\mathbf{V}_{SDLM}(q'_w)$ (m s^{-1}/°)	AT (q'_w)	$\mathbf{V}_{BT}$ (Saomai) (m s^{-1}/°)	$\mathbf{V}_{SDLM}(q'_b)$ (m s^{-1}/°)	AT (q'_b)
0000 7 Sep	4.4/306	4.8/301	0.4/−5	1.07	2.3/212	−0.02	5.2/327	1.11	1.0/355	0.16	7.1/316	2.5/046	0.00
1200 7 Sep	7.6/292	6.2/294	−1.4/2	0.82	2.8/218	0.09	6.2/319	0.72	1.0/349	0.07	6.1/292	2.5/041	−0.13
0000 8 Sep	7.3/288	6.8/295	−0.5/6	0.92	3.4/220	0.18	6.7/324	0.74	1.7/343	0.14	5.9/296	2.5/035	−0.07
1200 8 Sep	5.6/278	4.7/299	−0.9/21	0.79	3.0/217	0.27	5.2/334	0.52	2.0/337	0.18	6.0/307	1.7/034	0.02
0000 9 Sep	3.5/234	2.9/255	−0.6/21	0.77	4.2/210	1.11	3.0/347	−0.34	1.9/337	−0.11	5.1/311	1.3/025	0.08
1200 9 Sep	5.1/221	4.8/215	−0.3/−6	0.94	4.8/191	0.82	1.9/292	0.12	1.3/341	−0.12	5.6/317	2.0/014	0.20
0000 10 Sep	5.7/205	5.4/197	−0.3/−8	0.93	6.6/171	0.98	2.8/302	−0.05	1.5/349	−0.21	5.7/294	1.6/355	0.14
1200 10 Sep	5.5/190	4.7/165	−0.8/−26	0.76	7.8/160	1.22	3.2/332	−0.45	1.2/359	−0.22	2.5/288	1.2/339	0.32
0000 11 Sep	3.9/176	5.7/140	1.8/−37	1.18	8.6/145	1.90	3.0/335	−0.72	1.1/011	−0.28	3.5/306	1.2/327	0.31
1200 11 Sep	4.9/143	5.5/123	0.6/−19	1.06	8.4/133	1.67	3.0/330	−0.61	0.7/018	−0.08	3.4/297	0.7/316	0.21
0000 12 Sep	7.8/104	9.5/101	1.7/−3	1.41	10.4/114	1.31	2.5/357	−0.09	0.5/026	0.01	3.1/295	0.8/304	0.26
Mean			−0.03/−5	0.97									
Std dev			1.04/18	0.20									

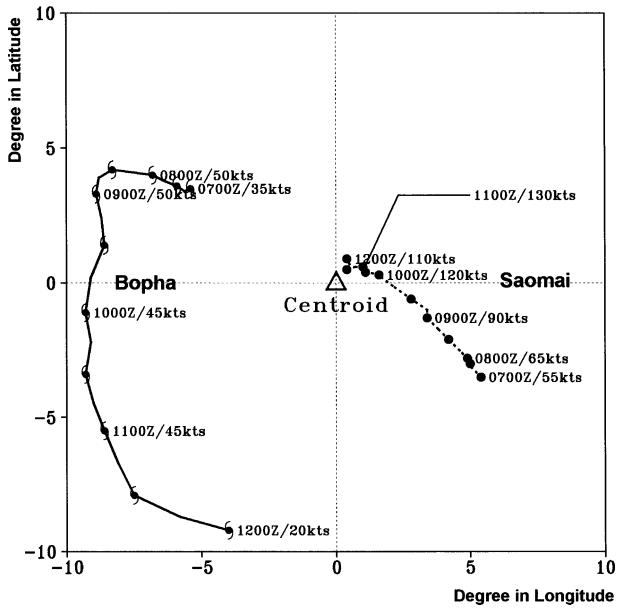

FIG. 10. Centroid-relative tracks of Bopha (in TC symbol) and Saomai (in solid dot) for every 12 h from 0000 UTC 7 Sep to 0000 UTC 12 Sep 2000.

of each vortex. However, for vortices of real tropical cyclones, it is not clear how to define an appropriate centroid that can best describe the relative motion of the binary vortices. Because Saomai was much stronger (see the intensity of each storm shown in Figs. 2 and 3) and broader (see Figs. 3 and 4), it is expected that the track of Bopha would be more affected by the binary interaction. In other words, the centroid should be weighted closer to the center of Saomai than to that of Bopha.

To better indicate the binary interaction processes, here we propose to define the centroid as the location weighted according to the strength of the steering flow induced by the PV perturbation associated with each storm, that is, the steering flow on Bopha associated with Saomai (q'_s) is $\mathbf{V}_{SDLM}(q'_s)$, and the steering flow on Saomai associated with Bopha (q'_b) is $\mathbf{V}_{SDLM}(q'_b)$. Therefore, the centroid position ($\mathbf{r}_c$) is thus defined as (see Fig. 9)

$$\mathbf{r}_c = \frac{|\mathbf{V}_{SDLM}(q'_b)|}{|\mathbf{V}_{SDLM}(q'_s)| + |\mathbf{V}_{SDLM}(q'_b)|}\mathbf{r}_b + \frac{|\mathbf{V}_{SDLM}(q'_s)|}{|\mathbf{V}_{SDLM}(q'_s)| + |\mathbf{V}_{SDLM}(q'_b)|}\mathbf{r}_s,$$

where $\mathbf{r}_b$ and $\mathbf{r}_s$ are the position vectors of Bopha and Saomai, respectively.

As shown in Fig. 10, it is clear that sustaining a distance of about 1200 km, Bopha and Saomai rotated cyclonically around each other, while the centroid is much closer to Saomai. Figure 10 succinctly reveals

how Bopha and Saomai mutually interacted. The unusual southward drift of Bopha appears to agree with the proposed mechanism as the direct binary interaction with one-way influence (Carr et al. 1997). We believe that the above PV analysis can nicely quantify the binary interaction processes, and the newly defined centroid-relative track can be isolated to describe the appropriate interaction of the TCs.

4. Summary

Tropical Storm Bopha (2000) showed a very unusual southward course parallel to the east coast of Taiwan, mainly steered by the circulation associated with Supertyphoon Saomai (2000) to Bopha's east. The binary interaction between the two typhoons is well demonstrated by the potential vorticity diagnosis. The quantitative description of the Fujiwhara effect is not easy for real-case tropical cyclones because such an effect on steering usually tends to be masked by other environmental steering flow. With the use of the piecewise PV inversion, this paper quantitatively evaluates how Bopha moved southward due to the circulation associated with Saomai, how the flow field associated Bopha steered Soamai, and how a still farther TC, Wukong, affected the motion of Bopha.

In summary, the detailed analysis in this study quantifies (see Table 1) that 1) the motion of Bopha is in agreement with the steering flow induced from the PV inversion; 2) the influence of Bopha on Saomai and Wukong on Bopha are both considerably smaller than the influence of Saomai on Bopha. Therefore it is concluded that there is a clear one-way binary interaction, namely, the presence of Saomai plays the major role in leading to the southward movement of Bopha.

A new centroid-relative track is proposed, with the position weighting based on the induced steering flow due to the PV anomaly of another storm. Note that such an analysis can be used to understand the more complicated vortex merging and interacting processes between/among multiple tropical cyclones either from observational data or specifically designed numerical experiments. Overall, in this paper we have clearly shown how the motion of Bopha was affected by the presence of Saomai. As the binary interaction can affect the behavior of close-by tropical cyclones, the results from such quantitative diagnosis of binary interaction can also shed some light on the improvement of the prediction of multiple nearby tropical cyclones, namely such PV inversion concept can be applied to real-time analysis and prediction system, and to quantitatively evaluate the impact of nearby storms.

Acknowledgments. The authors would like to thank two anonymous reviewers for helpful comments. Constructive discussions with Yuqing Wang are appreciated. Editorial assistance from Andrea Chin and data support from Kang-Ning Huang of Central Weather Bureau are also acknowledged. The research is supported by Grants NSC 90-2111-M-002-017 and NSC 90-2625-Z-002-004.

REFERENCES

Arakawa, A., and W. H. Schubert, 1974: Interaction of a cumulus cloud ensemble with the large-scale environment, Part I. *J. Atmos. Sci.,* **31,** 674–701.

Brand, S., 1970: Interaction of binary tropical cyclones of the western North Pacific Ocean. *J. Appl. Meteor.,* **9,** 433–441.

Carr, L. E., III, and R. L. Elsberry, 1998: Objective diagnosis of binary tropical cyclone interactions for the western North Pacific basin. *Mon. Wea. Rev.,* **126,** 1734–1740.

——, M. A. Boother, and R. L. Elsberry, 1997: Observational evidence for alternate modes of track-altering binary tropical cyclone scenarios. *Mon. Wea. Rev.,* **125,** 2094–2111.

Chan, J. C. L., and W. M. Gray, 1982: Tropical cyclone movement and surrounding flow relationship. *Mon. Wea. Rev.,* **110,** 1354–1376.

Chang, S. W. J., 1983: A numerical study of the interaction between two tropical cyclones. *Mon. Wea. Rev.,* **111,** 1806–1817.

——, 1984: Reply. *Mon. Wea. Rev.,* **112,** 1646–1647.

Charney, J. G., 1955: The use of primitive equations of motion in numerical prediction. *Tellus,* **7,** 22–26.

Davis, C. A., 1992: Piecewise potential vorticity inversion. *J. Atmos. Sci.,* **49,** 1397–1411.

——, and K. A. Emanuel, 1991: Potential vorticity diagnostics of cyclogenesis. *Mon. Wea. Rev.,* **119,** 1925–1953.

DeMaria, M., and C. L. Chan, 1984: Comments on ''A numerical study of the interactions between two tropical cyclones.'' *Mon. Wea. Rev.,* **112,** 1643–1645.

Dong, K., and C. J. Neumann, 1983: On the relative motion of binary tropical cyclones. *Mon. Wea. Rev.,* **111,** 945–953.

Fujiwhara, S., 1921: The mutual tendency towards symmetry of motion and its application as a principle in meteorology. *Quart. J. Roy. Meteor. Soc.,* **47,** 287–293.

——, 1923: On the growth and decay of vortical systems. *Quart. J. Roy. Meteor. Soc.,* **49,** 75–104.

——, 1931: Short note on the behavior of two vortices. *Proc. Phys. Math. Soc. Japan. Ser. 3,* **13,** 106–110.

Gryanik, V. M., 1983: Dynamics of singular geostrophic vortices in a two-level model of the atmosphere (or ocean). *Bull. Acad. Sci. USSR, Atmos. Oceanic Phys.,* **19,** 171–179.

Holland, G. J., and G. S. Dietachmayer, 1993: On the interaction of tropical-cyclone-scale vortices. III: Continuous barotropic vortices. *Quart. J. Roy. Meteor. Soc.,* **119,** 1381–1398.

Hoskins, B. J., M. E. McIntyre, and A. W. Robertson, 1985: On the use and significance of isentropic potential-vorticity maps. *Quart. J. Roy. Meteor. Soc.,* **111,** 877–946.

Kuo, H.-C., G. T.-J. Chen, and C.-H. Lin, 2000: Merger of tropical cyclones Zeb and Alex. *Mon. Wea. Rev.,* **128,** 2967–2975.

Lander, M., and G. J. Holland, 1993: On the interaction of tropical-cyclone-scale vortices. I: Observations. *Quart. J. Roy. Meteor. Soc.,* **119,** 1347–1361.

Liou, C.-S., and Coauthors, 1997: The second-generation global forecast system at the Central Weather Bureau in Taiwan. *Wea. Forecasting,* **12,** 653–663.

Ritchie, E. A., and G. J. Holland, 1993: On the interaction of tropical-cyclone-scale vortices. II: Discrete vortex patches. *Quart. J. Roy. Meteor. Soc.,* **119,** 1363–1379.

Shapiro, L. J., 1996: The motion of Hurricane Gloria: A potential vorticity diagnosis. *Mon. Wea. Rev.,* **124,** 1497–2508.

——, and J. L. Franklin, 1999: Potential vorticity asymmetries and tropical cyclone motion. *Mon. Wea. Rev.,* **127,** 124–131.

Wang, Y., and G. J. Holland, 1995: On the interaction of tropical-

cyclone-scale vortices. IV: Baroclinic vortices. *Quart. J. Roy. Meteor. Soc.*, **121,** 95–126.

Wu, C.-C., and K. A. Emanuel, 1995a: Potential vorticity diagnostics of hurricane movement. Part I: A case study of Hurricane Bob (1991). *Mon. Wea. Rev.*, **123,** 69–92.

——, and ——, 1995b: Potential vorticity diagnostics of hurricane movement. Part II: Tropical storm Ana (1991) and Hurricane Andrew (1992). *Mon. Wea. Rev.*, **123,** 93–109.

——, and Y. Kurihara, 1996: A numerical study of the feedback mechanisms of hurricane–environment interaction on hurricane movement from the potential vorticity perspective. *J. Atmos. Sci.*, **53,** 2264–2282.